International Journal of Computer Assisted Radiology and Surgery manuscript No.
(will be inserted by the editor)

Deformable Registration of Pre-Operative MR, Pre-Resection Ultrasound and Post-Resection Ultrasound Images of Neurosurgery

Hassan Rivaz · **D. Louis Collins**

Received: date / Accepted: date

Abstract
Purpose Sites that use ultrasound (US) in image-guided neurosurgery (IGNS) of brain tumors generally have three sets of imaging data: pre-operative magnetic resonance (MR) image, pre-resection US, and post-resection US. The MR image is usually acquired days before the surgery, the pre-resection US is obtained after the craniotomy but before the resection, and finally the post-resection US scan is performed after the resection of the tumor. The craniotomy and tumor resection both cause brain deformation, which significantly reduces the accuracy of the MR-US alignment.

Method Three unknown transformations exist between the three sets of imaging data: MR to pre-resection US, pre- to post-resection US, and MR to post-resection US. We use two algorithms that we have recently developed to perform the first two registrations (i.e. MR to pre-resection US, and pre- to post-resection US). Regarding the third registration (MR to post-resection US), we evaluate three strategies. The first method performs a registration between the MR and pre-resection US, and another registration between the pre- and post-resection US. It then composes the two transformations to register MR and post-resection US; we call this method *compositional* registration. The second method ignores the pre-resection US and directly registers the MR and post-resection US; we refer to this method as *direct* registration. The third method is a combination of the first and second: it uses the solution of the compositional registration as an initial solution for the direct registration method. We call this method *group-wise registration*.

Results We use data from 13 patients provided in the MNI BITE database for all of our analysis. Registration of MR and pre-resection US reduces the average of the mean target registration error (mTRE) from 4.1 mm to 2.4 mm. Registration of pre- and post-resection US reduces the average mTRE from 3.7 mm to 1.5 mm. Regarding the registration of MR and post-resection US, all three strategies reduce the mTRE. The initial average mTRE is 5.9 mm, which reduces to: 3.3 mm with the compositional method, 2.9 mm with the direct technique, and 2.8 mm with the group-wise method.

Conclusion Deformable registration of MR and pre- and post-resection US images significantly improves their alignment. Among the three methods proposed for registering the MR to post-resection US, the group-wise method gives the lowest TRE values. Since the running time of all registration algorithms is less than 2 min on one core of a CPU, they can be integrated into IGNS systems for interactive use during surgery.

Keywords Non-rigid registration · intra-operative ultrasound · Brain surgery · Image guided neuro-surgery · IGNS

Hassan Rivaz(✉)
Department of Electrical and Computer Engineering
PERFORM Centre
Concordia University
1455 Maisonneuve west
Montreal, QC, H3G 1M8
Canada
E-mail: hrivaz@ece.concordia.ca

D. Louis Collins(✉)
McConnell Brain Imaging Centre (BIC)
Montreal Neurological Institute (MNI)
McGill University
3801 University Street
Montreal, QC, H3A 2B4
Canada
E-mail: louis.collins@mcgill.ca

1 Introduction

Each year, thousands of Canadians undergo neurosurgery for resection of lesions such as tumors in close proximity

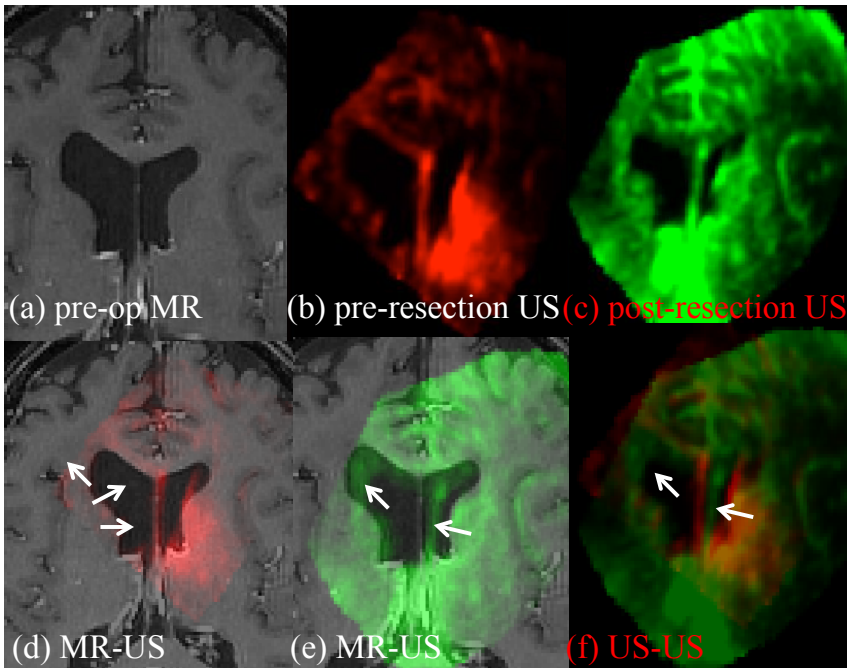

Fig. 1: MR and US images of neurosurgery. (a) is the pre-operative MR, and (b) and (c) are respectively pre- and post-resection US images. (d) shows a relatively good alignment between the MR and the pre-resection US. The arrows point to the ventricle boundary and septum. (e) shows that the alignment of MR and post-resection US is significantly degraded due to a large amount of brain deformation. (f) confirms that the deformation occurred during the resection is large, since there is a large misalignment between the pre- and post-resection US images.

to critical areas of the brain. While image-guided neurosurgery (IGNS) systems can be used to track surgical tools with respect to the pre-operative magnetic resonance (MR) images, movement of brain tissue during surgery invalidates the image-to-patient mapping and thus reduces the effectiveness of using pre-operative images for intra-operative surgical guidance. The movement of brain is caused by biochemical and physical factors, and is referred to as *brain shift* in the literature [1–4]. Some centers have used intra-operative MRI [5–9] and functional MRI [10] to address this issue. While the data acquired can yield exquisite anatomical and functional data [11], the system is expensive and cumbersome and requires major modifications to the operative room (OR) and surgical tools. Tracked intra-operative ultrasound (US), however, is inexpensive and does not require significant changes to the OR or operating procedure. In neurosurgery, intraoperative US has been used in imaging tumor resection and epilepsy surgery [12–20] and placement of cerebral ventricle catheters [21] for example.

This work focuses on image-guided resection of brain tumors. When US is used in these procedures, a first set of US is acquired after the craniotomy but before opening the dura to help the surgeon find the tumor and its boundaries, and other US acquisitions can be performed during the resection of the tumor. Fusion of the pre-operative MR and intra-operative US is of significant clinical value since many critical structures that have high contrast in the MR image are not well visualized in US. In addition, surgeons have more training in using and interpreting MR images. Furthermore, functional and vascular data, registered to the pre-operative MR are required during the surgery. To allow navigation based on the preoperative MR images, a standard patient registration procedure using a number of facial landmarks is performed. This landmark registration allows rigid registration of the MR to the patient space. Furthermore, the US probe is tracked, which allows the fusion of the US and MR images. Four main sources of error make this tracking-based navigation system inaccurate. First, there is an error associated with localizing the facial landmarks and registering them to the MR image. Second, the tracking system is not perfect, and therefore the location and orientation of the US probe is prone to error. Third, US calibration has errors, which means that the physical location of US images is slightly different from what the IGNS system assumes. Finally, due to brain shift, which can be as much as 50 mm [5] in some locations, the pre-operative MR images are no longer an accurate registration of the patent's anatomy, even after a perfect linear registration. To solve

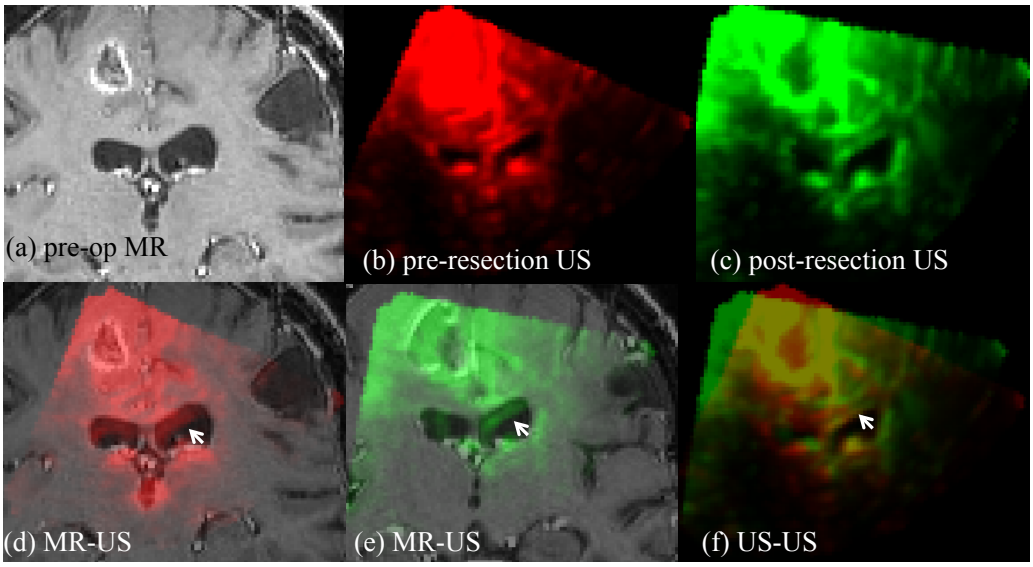

Fig. 2: MR and US images of neurosurgery. (a) is the pre-operative MR, and (b) and (c) are respectively pre- and post-resection US images. (d) shows that the brain deformation is large between the MR and the pre-resection US, as pointed to by the arrow. (e) shows that the deformation is large between the MR and the post-resection US. (f) shows that the deformation occurred during the resection is relatively low, as the two US images align well.

these problems, deformable registration of the MR and US image using the intra-operative US data is of high clinical importance.

Figure 1 shows the brain shift between MR and US images in a patient from the BITE database [22]. Part (d) shows that the alignment of MR and pre-resection US is relatively good (see septum pellucidum and ventricle boundary, which are identified by the arrows). However, the alignment degrades significantly between MR and post-resection US images as shown in (e). Looking at (f), we can confirm that most of the deformation has happened during the resection, since the alignment of the pre- and post-resection US images is relatively poor. Recent work has, in fact, studied the brain shift that happens after craniotomy and durotomy [23, 24].

Figure 2 shows images from another patient from the BITE database, which present different deformation patterns compared to Figure 1. The alignment in (d) is poor, which means that the initial patient-to-image registration based on skin markers was inaccurate or a large deformation has happened during the craniotomy. The deformation during the resection is, however, low, as shown in (f), where the pre- and post-resection ultrasound images align relatively well.

The registration of the MR to post-resection US is the most challenging task, compared to MR to pre-resection US and pre- to post-resection US registrations. We propose three strategies to perform this registration as follows.

1. We first perform a registration between the MR and pre-resection US, followed by a second registration between the pre- and post resection US images. These two registrations give us two transformations, which we compose to find the transformation between the MR and post-resection US.
2. We ignore the pre-resection US image and directly register the MR and post-resection US.
3. We combine the above two methods to perform a group-wise registration.

The advantage of the first method is that it performs two simpler registration tasks. The advantage of the second method is that it does not suffer from error accumulation, a well-known problem with all sequential tracking techniques [25] where incremental small errors can add to large values. The third method combines the advantages of the first two, and is therefore expected to outperform the other two. We show that all three techniques substantially improve the registration accuracy of MR and post-resection US compared to the linear skin landmark registration used to establish the initial patient-to-image registration.

We use two nonlinear registration techniques that we have recently developed: for registration of US images, we use REgistration of ultraSOUND volumes (RESOUND) algorithm [26], and for registration of MR and US volumes, we use Robust PaTch-based cOrrelation Ratio (RaPTOR) [27]. Previous work that has tackled registration of MR and US include the following. Roche et al. [28] performed a

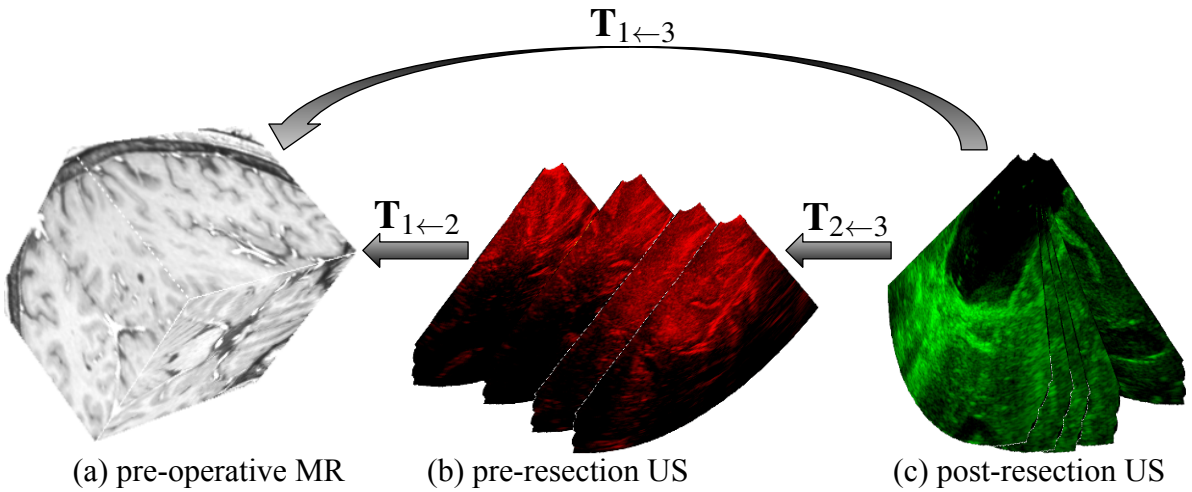

Fig. 3: The three transformations between the three MR and US volumes. More than 300 slices are acquired in both pre- and post-resection scans; we are only showing few here for better visualization.

parametric polynomial fit of US intensity as a function of MR and its gradient to construct a functional correlation ratio similarity metric. Arbel et al. [29] and Mercier et al. [19] segmented the MR image and assigned different intensity transformations to different MR regions to generate pseudo-US images. They then registered the pseudo-US to the real US using the ANIMAL registration technique of Collins et al. [30]. Using a similar approach, Kuklisova-Murgasova et al. [31] recently proposed to register MR to a segmented atlas, generate a US-like volume from the MR volume, and finally register it with the US volume using a uni-modal block-matching technique. Penney et al. [32] generated blood vessels probability maps from US and MR and registered these maps using cross correlation. Ji et al. [33], Hartov et al. [34] and Brooks et al. [35] used mutual information (MI) of US and MR, and Zhang et al. [36] performed phase-based MI.

The contributions of this work are summarized below. (1) We develop a *group-wise* registration algorithm that considers the MR volume and the two US volumes *simultaneously* to estimate the transformation between the MR and post-operative US volumes. We use the pair-wise registration algorithms of [26,27] to develop the group-wise algorithm. (2) We develop a compositional registration algorithm that composes sequential image transformations to calculate the deformable transformation between the MR and post-resection US volumes. (3) We compare the group-wise, compositional and direct registration approaches. We show that: (3a) The direct registration method does not produce optimal results if the amount of brain shift that occurs during craniotomy and tumor resection is high. (3b) The compositional registration method breaks solving for the large brain shift into two smaller ones that happen during craniotomy (registration of the MR and pre-resection US) and tumor resection (registration of the pre- and post-resection US). Therefore, it is robust against large total brain deformations, but suffers from error accumulation. (3c) Finally, we show that the group-wise algorithm combines the advantages of the compositional and direct strategies, and therefore produces robust and accurate estimations of the registration parameters in all cases.

This paper is organized as follows. We first elaborate on different registration techniques that we use for registering the MR and US images. We then provide extensive experiments and results to compare the performance of different registration methods, and suggest directions for future work.

2 Methods

There are three transformations between the three sets of MR, pre-resection US and post-resection US images, one transformation between each pair of images (see Figure 3). We annotate these transformations as follows:

1. MR and pre-resection US by $\mathbf{T}_{1\leftarrow 2}$
2. Pre- and post-resection US by $\mathbf{T}_{2\leftarrow 3}$
3. MR and post-resection US by $\mathbf{T}_{1\leftarrow 3}$

Due to brain deformation, we model all of these transformations using free-form cubic B-splines [37]. Calculation of $\mathbf{T}_{1\leftarrow 2}$ and $\mathbf{T}_{1\leftarrow 3}$ needs multi-modal registration, while estimation of $\mathbf{T}_{2\leftarrow 3}$ requires mono-modal registration of US images. We elaborate next on how we estimate these transformations.

2.1 Multi-modal Registration of MR and US Volumes

Performing registration between images of different modality, such as MR and US, is in general more challenging than mono-modal registration. Similarity metrics such as normalized cross correlation (NCC) do not usually work in this case because the intensity relationship between two images is complex. We proposed Robust PaTch-based cOrrelation Ratio (RaPTOR) in [27], which uses correlation ratio (CR) as the similarity metric for each small patch and averages the result over N_p patches to estimate RaPTOR:

$$\text{RaPTOR}(I_{MR}, I_{US}) = D(I_{MR}, I_{US}) = \frac{1}{N_p} \sum_{i=1}^{N_p} (1 - \eta_i(I_{MR} \mid I_{US})) \tag{1}$$

where I_{MR} and I_{US} are respectively MR and US images and $\eta_i(I_{MR} \mid I_{US})$ is their correlation ratio at the i^{th} patch. The registration in RaPTOR is done hierarchically in three levels to speed the computations and prevent the algorithm from getting trapped in local minima. At the two coarse levels, an approximate transformation is calculated that brings the volumes closer to alignment. In the final level, an accurate transformation that aligns the volumes is calculated using the approximate transformation.

RaPTOR is a *dissimilarity* metric between I_{MR} and I_{US} that varies between 0 and 1: for aligned images with functional intensity relationships, its value is close to 0. CR assumes a non-linear functional relationship between corresponding intensities, and along with mutual information (MI) is commonly used for multi-modal registration. Using efficient optimization techniques based on analytic gradients of the CR, RaPTOR performs non-rigid volumetric registration in about 30 sec on a single core of a 3.6 GHz processor. We use this algorithm to estimate $\mathbf{T}_{1\leftarrow 2}$. This algorithm is also used to estimate $\mathbf{T}_{1\leftarrow 3}$ by *directly* registering the MR and post-resection US images (i.e. ignoring the intermediate pre-resection US image).

2.2 Mono-modal Registration of US Volumes

We proposed non-rigid REgistration of ultraSOUND volumes (RESOUND) algorithm in [26], which optimizes a regularized cost function with normalized cross correlation (NCC) as the similarity metric. NCC assumes a linear relationship between corresponding intensity values, and therefore is robust to linear intensity distortions. RESOUND averages squared NCC estimations over N_p small patches:

$$\text{RESOUND}(I_{MR}, I_{US}) = D(I_{MR}, I_{US}) = -\frac{1}{N_p} \sum_{i=1}^{N_p} \rho_i^2(I_{MR}, I_{US}) \tag{2}$$

where $\rho_i(I_{MR}, I_{US})$ is the NCC value between the MR and US images in the i^{th} patch. Similar to RaPTOR, the registration in RESOUND is done hierarchically in three levels. RESOUND is also a *dissimilarity* metric that varies between 0 and 1. RESOUND also uses robust estimation techniques that suppress outliers and missing data. It further exploits efficient stochastic gradient descent optimization, which allows it to perform nonlinear registration between volumetric data in about 5 sec on a single core of a 3.6 GHz processor. We use this algorithm to estimate a cubic B-spline deformation field for $\mathbf{T}_{2\leftarrow 3}$.

2.3 Compositional Registration for Estimating $\mathbf{T}_{1\leftarrow 3}$

There are three main difficulties in computing $\mathbf{T}_{1\leftarrow 3}$: (1) the amount of brain shift is generally highest between the pre-operative MR and post-resection US, (2) the images are of different modality, and (3) the tumor in the MR image is replaced by the tumor cavity in the post-resection US image, a region which should be treated as outlier data. Compositional estimation of this transformation breaks this difficult task into the two easier tasks of calculating $\mathbf{T}_{1\leftarrow 2}$ and $\mathbf{T}_{2\leftarrow 3}$: (1) the deformation is smaller in each transformation, (2) the difficult multi-modal registration is now performed on MR and pre-resection US images, which are more similar spatially compared to the MR and post-resection US and (3) the outlier suppression should be performed on a relatively easier mono-modal registration of US images. The disadvantage is that the errors in estimation of $\mathbf{T}_{1\leftarrow 2}$ and $\mathbf{T}_{2\leftarrow 3}$ can be accumulated into $\mathbf{T}_{1\leftarrow 3}$. We therefore propose the group-wise method in the next section.

2.4 Group-wise Estimation of $\mathbf{T}_{1\leftarrow 3}$

By combining the direct and compositional approaches, we propose a group-wise technique to estimate $\mathbf{T}_{1\leftarrow 3}$. Our motivation is that this combination should eliminate the accumulation of error in the compositional technique. Here, we first compose $\mathbf{T}_{1\leftarrow 2}$ and $\mathbf{T}_{2\leftarrow 3}$ transformations to get an estimate for $\mathbf{T}_{1\leftarrow 3}$. We then use this estimate as the initial guess for direct registration of the MR and post-resection US. Therefore, this step is more straightforward due to the availability of a relatively accurate estimate of the transformation, while it eliminates the error accumulations of the compositional registration step.

Fig. 4: The pre-resection US images are acquired while the probe is tracked in 3D. The tracking data is then used to reconstruct a 3D volume from 2D US slices.

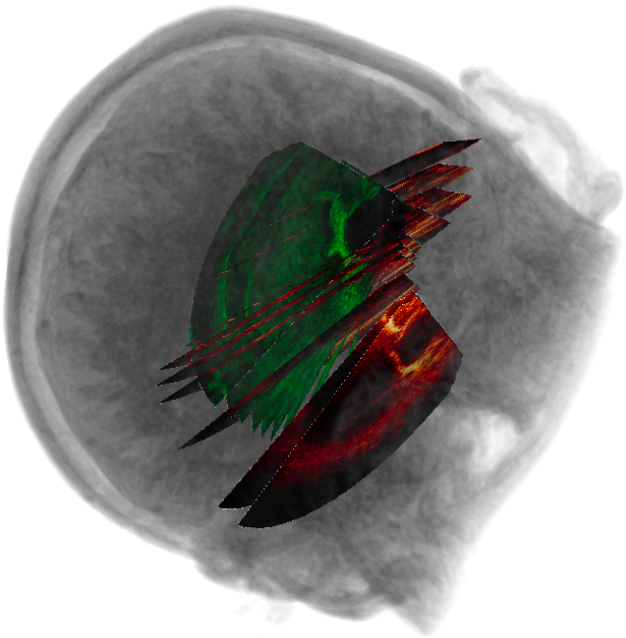

Fig. 5: The pre- and post-resection US slices (respectively in red and green) shown on the rendered pre-operative MR volume. US slides are transformed into the MR coordinate system using the tracking data from the Polaris system. More than 300 US slides are collected in either scans; we are only showing few here for improved visualization.

3 Experiments

3.1 Data Description

The clinical data from image guided neuro-surgery is obtained from 13 patients with gliomas in the Montreal Neurological Institute. The study was approved by the Montreal Neurological Institute and Hospital Review Ethics Board, and informed consent from each participant was received. The data is available online from `http://www.bic.mni.mcgill.ca/BITE`. The pre-operative MR images are gad-enhanced T1 weighted and are acquired a few days before the surgery. The intra-operative US images are obtained using an HDI 5000 (Philips, Bothell, WA) ultrasound machine with a P7-4 MHz phased array transducer. Full description of the data is provided in [22]. The ultrasound probe is tracked using a Polaris camera (NDI, Waterloo, Canada), and 3D US volumes are reconstructed using the tracking information. Figure 4 shows the US probe during data acquisition with the tracking markers.

We use the tracking information to perform a rigid initial alignment of US images to the MR volume. Figure 5 shows the pre- and post-operative US slices relative to the rendered MR volume. We reconstruct US volumes with a pixel size of 1 mm in the $x\,y\,z$ directions. This relatively large pixel size means that for every pixel, multiple US measurements from different images at different angles are available. Therefore, the effect of US speckle is minimized, since the US speckle pattern changes when imaged from different angles [38]. Each volume has a different size because the depths and sweeping areas are different; the typical size is approximately 100^3 voxels. We resample the MR volume to the same isotropic 1 mm pixel size.

3.2 Landmark Selection and mTRE Estimation

To validate the results, three experts have selected corresponding anatomical landmarks in US and MR images [39, 22]. For this task, US and MR images are sampled at the small 0.3 mm voxel size in all dimensions. The landmarks are selected independently by all the three experts throughout the volumes in three orthogonal planes. The landmarks are used to calculate mean target registration error (mTRE). The mTRE of n corresponding marks at locations $\mathbf{x}$ and $\mathbf{x}'$ in the two images is calculated according to

$$\text{mTRE} = \frac{1}{n}\sum_{i}^{n} \|\mathbf{T}(\mathbf{x}_i) - \mathbf{x}'_i\| \tag{3}$$

where $\mathbf{T}$ is one of the three transformation in Figure 3 and $\|\mathbf{v}\|$ is the length of the vector $\mathbf{v}$. Lower mTRE indicates a more accurate alignment.

3.3 Statistical Tests

Two types of tests are commonly used for statistical hypothesis testing: a t-test for normally distributed populations, and Wilcoxon signed-rank test for data that is not Gaussian. Our experiments showed that the TRE estimates in IGNS are not

normally distributed (see Figure 7 for example), and therefore we use the Wilcoxon signed-rank test for estimating the p-value of statistical significance.

4 Results

In this section, we first provide images that show the pattern of the brain shift during the craniotomy and tumor resection. We then present quantitative mTRE results of different registration methods.

4.1 Qualitative Brain Shift Estimation

Figure 6 demonstrates how different transformations are estimated. The MR and pre- and post-resection US images are overlaid with the blue contours to help the reader visually identify homologous structures between the different images. The contours are estimated automatically from the MR image. We first use RaPTOR to estimate $\mathbf{T}_{1\leftarrow 2}$; the magnitude of the brain shift corresponding to the US image of (b), i.e. $\mathbf{S}_{1\leftarrow 2}$, is shown in (d). Using RESOUND, we estimate $\mathbf{T}_{2\leftarrow 3}$ and calculate the brain shift $\mathbf{S}_{2\leftarrow 3}$ magnitude in (e). In (f) to (h), we estimate $\mathbf{S}_{1\leftarrow 3}$ using three different methods: direct in (f), compositional in (g), and group-wise in (h). We see that the brain shift value is the largest around the resection is approximately 20 mm.

4.2 mTRE Results of the Compositional Method

To estimate $\mathbf{T}_{1\leftarrow 3}$ using the compositional approach, we first use RaPTOR to estimate $\mathbf{T}_{1\leftarrow 2}$. Using the landmarks provided in the BITE database [19], we quantify the registration accuracy (see Table 1). The initial mean mTRE is 4.1 mm, which is reduced to 2.4 mm after the registration.

We then use RESOUND to estimate $\mathbf{T}_{2\leftarrow 3}$. The mTRE values before and after the registration are shown in Table 1. Because the tumor volume is outlier data, we also report its size in the second column. We see that despite the large outlier data, RESOUND has reduced the mTRE from 3.7 mm to 1.5 mm. In Table 1, we note that the average initial mTRE values are respectively 4.1 mm and 3.7 mm. Since mTRE is an indication for brain shift, this suggests that the deformations that happen during craniotomy (i.e. $\mathbf{T}_{1\leftarrow 2}$) and during resection (i.e. $\mathbf{T}_{2\leftarrow 3}$) are in average similar. Nonetheless, this is not the case for all patients: for patient 1, the mTRE values from Table 1 are respectively 6.3 mm and 2.3 mm, while for patient 3 the mTRE values are 2.5 mm and 4.6 mm.

Having calculated $\mathbf{T}_{1\leftarrow 2}$ and $\mathbf{T}_{2\leftarrow 3}$, we now compose them to obtain $\mathbf{T}_{1\leftarrow 3}$. The mTRE results are shown in the fourth column of Table 2. The initial average mTRE value of 5.9 mm is substantially reduced to 3.3 mm using this technique. The maximum TRE is also reduced greatly from 14.0 mm to 4.8 mm. Furthermore, the reduction in mTRE value is statistically significant, with a p-value of 0.002.

4.3 mTRE Results of the Direct Method

We use the robust multi-modal registration algorithm of RaPTOR to directly estimate $\mathbf{T}_{1\leftarrow 3}$. The results are presented in the fifth column of Table 2: the average mTRE and maximum TRE values are substantially reduced to 2.9 mm and 4.4 mm respectively. Furthermore, the improvement in mTRE is statistically significant with a p-value of 0.0002. The large mTRE and maximum TRE values of relatively 14.0 mm and 17.0 mm in patient 11 show the large capture range of RaPTOR. A large capture range is important to ensure that the algorithm does not diverge, or converge to an incorrect minima, for cases with large initial misalignment of MR and US images.

4.4 mTRE Results of the Group-wise Method

Finally, we use the compositional $\mathbf{T}_{1\leftarrow 3}$ results of Section 4.2 as an initial solution and perform direct registration between the MR and post-resection US images. The mTRE results are summarized in the last column of Table 2: the average mTRE and maximum TRE values are substantially reduced to 2.8 mm and 4.1 mm respectively. Furthermore, the improvement in mTRE is statistically significant with a p-value of 0.0002. Using a paired Wilcoxon test on the magnitude of the registration residuals, we find no statistical difference between the compositional and direct methods (p=0.24), a significant improvement of the group-wise method over the compositional method (p=0.008) and a trend to improvement of the groupwise method over the direct method (p = 0.056).

The *accuracy* and *robustness* of a registration algorithm are both critical in its successful clinical translation. The accuracy is usually measured using mTRE values; the results of Table 2 show that the direct and group-wise methods have the smallest average mTRE values. The robustness of a method can be evaluated by assessing its performance against large initial misalignments; the highest initial TRE is 17.0 mm in P11, which is reduced to 6.9 mm, 8.1 mm and 5.2 mm using respectively compositional, direct and group-wise methods. This result is in fact very intuitive: the compositional method deals with smaller deformation since it breaks the large deformation estimation problem into two smaller ones. Therefore, it outperforms the direct method when the initial misalignment is large. However, it suffers from error accumulation as a result of composing transformations. The group-wise method exploits the advantages of both compositional and direct methods, and is therefore

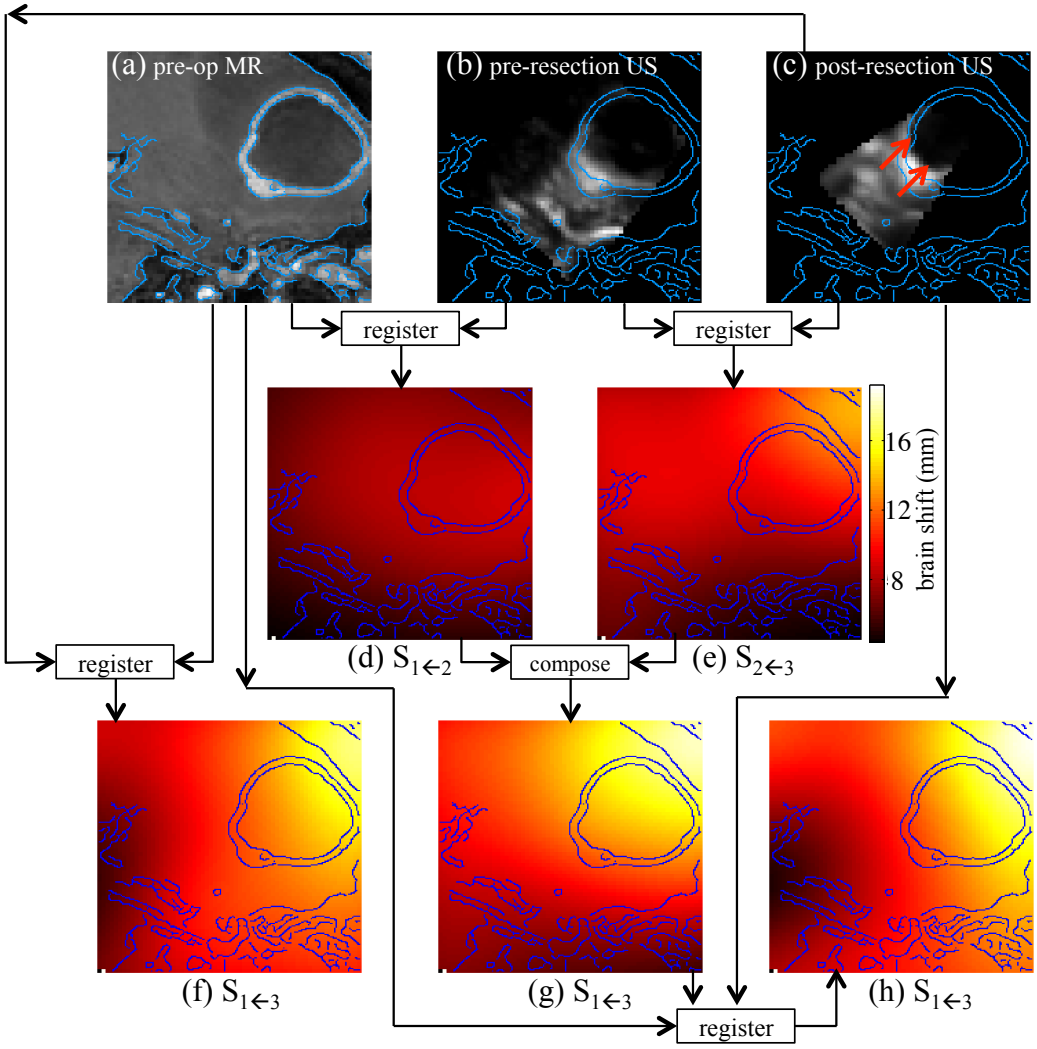

Fig. 6: The brain shift estimation between volumes acquired at different times. (a) to (c) shows the pre-operation MR, pre-resection US and the post resection US respectively. The arrows in (c) point to the tumor cavity. The blue contour shows MR edges and is superimposed on all figures to help readers with visual comparison. (d) shows the brain shift between (a) and (b), and (e) shows the brain shift between (b) and (c). The total brain shift between (a) and (c) is computed with three different methods in (f) to (h) as shown, which are similar as expected. (f) is the direct method, (g) is the compositional method, and (h) is the group-wise method. Note that all registrations are done in 3D.

the most accurate *and* robust approach. The *p*-values of the paired Wilcoxon tests of the maximum TRE of the group-wise method compared to the initial values and compose and direct registrations are respectively 0.0002, 0.0017, 0.0017 and 0.039, all statistically significant.

The box plot of Figure 7 allows easy comparison of the initial TRE values with the three registration methods. We see that the direct registration method outperforms the compositional technique, which means that the accumulation of error is an important factor. The group-wise method gives the best TRE results. We believe the reason for improved performance of the group-wise method, compared to the direct method, is that the direct method can get trapped in a local minima if the misalignment is too large in some image regions. The compositional approach brings the images closer to alignment in such regions, reducing the risk of convergence to an incorrect local minima.

5 Discussion

The registration of MR and US is challenging due to numerous reasons. In MR, the intensity of every voxel reflects the proton density modulated by the magnetic properties of that tissue, and hence MR images tissue type. In contrast,

	MR & pre-resection US ($\mathbf{T}_{1\leftarrow 2}$)			pre- & post-resection US ($\mathbf{T}_{2\leftarrow 3}$)		
Patient	Landmarks	Initial	RaPTOR	Tumor size (cm^3)	Initial	RESOUND
P1	35	6.3 (1.9-9.1)	**1.8** (0.4-5.4)	79.2	2.3 (0.6-5.4)	**1.8** (0.5-4.0)
P2	40	9.4 (6.3-14.6)	**4.2** (0.5-9.8)	53.7	3.9 (2.8-5.1)	**1.4** (0.7-2.3)
P3	32	3.9 (1.0-6.1)	**1.7** (0.5-3.3)	31.6	4.6 (3.0-5.9)	**1.4** (0.7-2.2)
P4	31	2.6 (0.5-6.9)	**2.0** (0.3-5.8)	0.2	4.1 (2.6-5.5)	**1.2** (0.3-2.4)
P5	37	2.3 (0.2-4.4)	**1.8** (0.5-4.0)	32.3	2.3 (1.4-3.1)	**1.0** (0.2-1.7)
P6	19	3.0 (0.3-6.3)	**2.5** (0.6-6.2)	13.9	4.4 (3.0-5.4)	**1.0** (0.4-1.7)
P7	23	3.8 (0.0-8.5)	**2.7** (0.8-5.7)	63.1	2.7 (1.7-4.1)	**1.7** (0.9-3.6)
P8	21	5.1 (2.5-7.6)	**2.5** (0.6-6.7)	4.8	2.2 (1.0-4.6)	**1.4** (0.6-3.2)
P9	25	3.0 (0.8-5.3)	**1.7** (0.3-3.0)	10.4	3.9 (1.0-6.7)	**1.9** (0.7-4.1)
P10	25	1.5 (0.6-3.5)	**1.4** (0.6-3.1)	39.7	2.9 (0.8-9.0)	**2.2** (0.6-5.3)
P11	21	3.7 (0.9-7.0)	**2.2** (1.1-4.2)	49.1	10.5 (7.8-13.0)	**2.5** (1.1-4.2)
P12	23	5.2 (1.5-10.4)	**3.8** (0.8-8.3)	31.9	1.6 (1.3-2.2)	**0.7** (0.2-1.6)
P13	23	3.8 (1.2-5.7)	**2.7** (0.7-5.2)	37.3	2.2 (0.6-4.0)	**1.3** (0.2-2.8)
mean	27	4.1 (1.4-7.3)	**2.4** (0.6-5.5)	34.4	3.7 (2.1-5.7)	**1.5** (0.5-3.0)
std	6.9	2.0 (2.7-2.9)	**0.8** (0.2-2.0)	23.3	2.4 (1.9-2.8)	**0.5** (0.3-1.1)

Table 1: The mean and range of TRE values (in mm) between the MR and pre-resection US volumes. RaPTOR is used here to estimate $\mathbf{T}_{1\leftarrow 2}$. The minimum value of each row is in bold font. 10 landmarks are selected in all 13 datasets of pre- and post-resection US volumes. The results of the last column are from [26].

US images the variations in the acoustic impedance of different tissue types, and therefore MR and US images intensities are widely different. In addition, spatial variations of the US image intensities are very high due to wave attenuation and scattering. We therefore used the RaPTOR algorithm for MR-US registration, which uses a local similarity metric based on statistical and information theoretic measures.

The presence of outliers in pre-operative MR to post-operative US registration further complicates MR to US registration. We therefore proposed three pair-wise and group-wise approaches to register these two volumes. The group-wise technique is a combination of RESOUND and RaPTOR algorithms, and is more computationally expensive compared to the pair-wise methods. Nevertheless, due to the efficient stochastic gradient decent optimization strategies, it runs in less than 2 min. This time includes the two registrations performed to find $\mathbf{T}_{1\leftarrow 2}$ and $\mathbf{T}_{2\leftarrow 3}$, the time needed to compose these two transformations, and the final registration to refine $\mathbf{T}_{1\leftarrow 3}$.

Our validation was based on real patient data using manually selected homologous landmarks. While the complexity of this data challenged our algorithms, there is an inherent uncertainty in manual landmark selection. In addition, although the landmarks cover most of the volumes and their number is large, some regions can be unrepresented in mTRE estimation. Therefore, qualitative study of the brain shift (such as in Figure 6) is an essential complement to the quantitative mTRE analysis.

Two factors are critical in determining the outcome of tumor resection surgery: the completeness of the resection while minimizing damage to healthy tissues. Accurate registration of the intra-operative US and pre-operative MR is significant in both fronts. It can help the surgeon accurately identify the safety zone, knowing that the intra- and post-resection scans enables identification of residual tumor. The results of Table 2 show that all three methods significantly reduce the mTRE errors. Among the three, the direct and group-wise methods give the smallest average mTRE values of respectively 2.9 mm and 2.8 mm. Another important factor is the robustness of the technique against large initial misalignments. The registration results of P11, which has the largest initial mTRE, show that the maximum TRE values of the direct and group-wise methods are respectively 8.1 mm and 5.2 mm, showing that the group-wise method is significantly more robust. The results of Figure 7 visually show the same behavior (see the last four columns that show the maximum TRE values): the group-wise method is significantly more robust in giving the smallest maximum TRE values.

It is informative to summarize the advantages and disadvantages of previous work that has also tackled MR and US registration, and provide a comparison to this work. The work of Roche et al. [28] is unique in that it uses both the intensity and gradient of MR to estimate the correlation ratio. Utilizing more information from the MR image can significantly improve the results. A disadvantage of this work is that a polynomial functional relationship is assumed between MR and US intensities, and therefore an interesting

Patient	Landmarks	Initial	Compose	Direct	Group-wise
P1	13	7.2 (5.2-10.6)	**3.6** (1.3-5.8)	3.8 (2.1-5.7)	3.7 (1.6-5.6)
P2	11	8.9 (6.2-13.8)	4.8 (1.7-9.4)	4.1 (1.7-8.3)	**4.0** (1.8-7.0)
P3	19	8.7 (6.6-12.7)	2.2 (1.4-3.3)	2.9 (0.9-6.9)	**2.1** (0.9-3.4)
P4	20	4.6 (1.1-11.3)	**2.5** (0.5-6.5)	2.5 (1.0-6.8)	2.5 (1.1- 6.0)
P5	21	3.6 (0.4-5.6)	**2.5** (0.4-4.8)	2.5 (0.9-4.1)	2.6 (1.0-4.1)
P6	16	3.6 (1.4-7.9)	3.5 (0.8-6.0)	2.5 (0.4-5.4)	**2.4** (0.4-5.3)
P7	17	6.4 (3.6-7.9)	5.4 (2.7-7.5)	**2.7** (1.5-5.4)	2.9 (1.9-6.5)
P8	15	5.1 (1.3-8.3)	2.9 (0.4-6.2)	2.5 (0.4-6.8)	**2.4** (0.4-6.4)
P9	12	4.2 (2.4-6.5)	1.9 (0.8- 4.8)	2.3 (0.5-5.2)	**1.8** (0.5-4.3)
P10	16	2.3 (0.2-4.6)	2.5 (0.3-5.6)	**1.6** (0.4-3.3)	1.7 (0.4-3.5)
P11	9	14.0 (11.8-17.0)	4.2 (1.1-6.9)	4.4 (1.8-8.1)	**3.9** (1.3-5.2)
P12	13	4.6 (1.7-7.1)	3.9 (2.2-6.6)	3.9 (2.1-6.1)	**3.8** (2.0-6.0)
P13	12	3.8 (2.1-7.0)	3.0 (1.0-4.9)	2.5 (1.1-4.9)	**2.5** (1.1-4.8)
mean	15	5.9 (3.4-9.3)	3.3 (1.1-6.0)	2.9 (1.1-5.9)	**2.8** (1.1-5.3)
max	21	14.0 (11.8-17.0)	4.8 (2.7-9.4)	4.4 (2.1-8.3)	**4.0** (2.0 7.0)
std	3.7	3.2 (3.3-3.6)	1.1 (0.7-1.5)	0.8 (0.6-1.4)	**0.8** (0.6-1.3)
p-value	-	-	0.002	**0.0002**	**0.0002**

Table 2: The mean and range of TRE (in mm) between the MR and post-resection US image. Second column shows the number of landmarks. Three methods are used here to estimate $\mathbf{T}_{1\leftarrow 3}$. The smallest number in every row is in bold. The p-values in the last row show the statistical significance of improvement over the initial mTRE. Also see Figure 7. The results of the fifth column are from [27].

area of future work is to extend this method to the estimation of nonparametric functional relationship. The work of Arbel et al. [29], Mercier et al. [19] and Kuklisova-Murgasova et al. [31] transform the multi-modal registration problem to a uni-modal one, and hence enables the use of well-established and computationally efficient uni-modal registration methods. A disadvantage is that the presence of pathology can render US simulation from the MR volume challenging. A big advantage of the work of Ji et al. [33], Hartov et al. [34] and Brooks et al. [35] is that they use MI, a well-established similarity metric that has been rigorously tested. A drawback is that MI assumes that the intensity relations between the two modalities is the same throughout the two volumes, and therefore is susceptible to the large spatial intensity variations in the US images. It is also computationally expensive. Our work is unique in that it addresses the problem of registering post-resection US to pre-operative MR. In addition, we take advantage of the information in the pre-resection US image and use it to improve the registration results. By utilizing the pre-resection US image in the group-wise registration of MR and post-resection US, we are breaking the hard registration problem of estimating a large deformation between two images of different modality with outliers into two simpler problems: estimation of $\mathbf{T}_{1\leftarrow 2}$ requires multi-modal registration without outliers with relatively small deformations, and estimation of $\mathbf{T}_{2\leftarrow 3}$ needs an easier uni-modal registration with outliers. Finally, we use efficient stochastic gradient-based optimization techniques, and hence the running time of our algorithms is under 2 min for volumetric data.

The deformable image registration techniques presented in this work significantly improves the alignment between US and MR images, which results in improved confidence in the neuronavigation system, and can potentially reduce surgical time and complications. In future work, we will analyze a larger series of patient data, and will study how often the improved image alignment leads to a change in the surgical plan. In addition, we will apply the techniques developed in this work to other operations in the brain that are subject to brain shift.

6 Conclusions

Three sets of images are commonly available in IGNS: pre-operative MR, pre-resection US and post-resection US. We performed nonlinear registration of MR to pre-resection US, pre- to post-US, and MR to post-resection US. For the most challenging problem of MR to post-resection US, we proposed three approaches: compositional, direct and group-wise. We showed that the group-wise algorithm gives the best results, reducing the average mTRE over 13 patients from 5.9 mm to 2.8 mm, and the maximum TRE from 17.0 mm to 7.0 mm. The computational time of all of these non-rigid volumetric registration methods is less than 2 min on a single CPU core. Therefore, these methods are highly suitable for integration within IGNS systems.

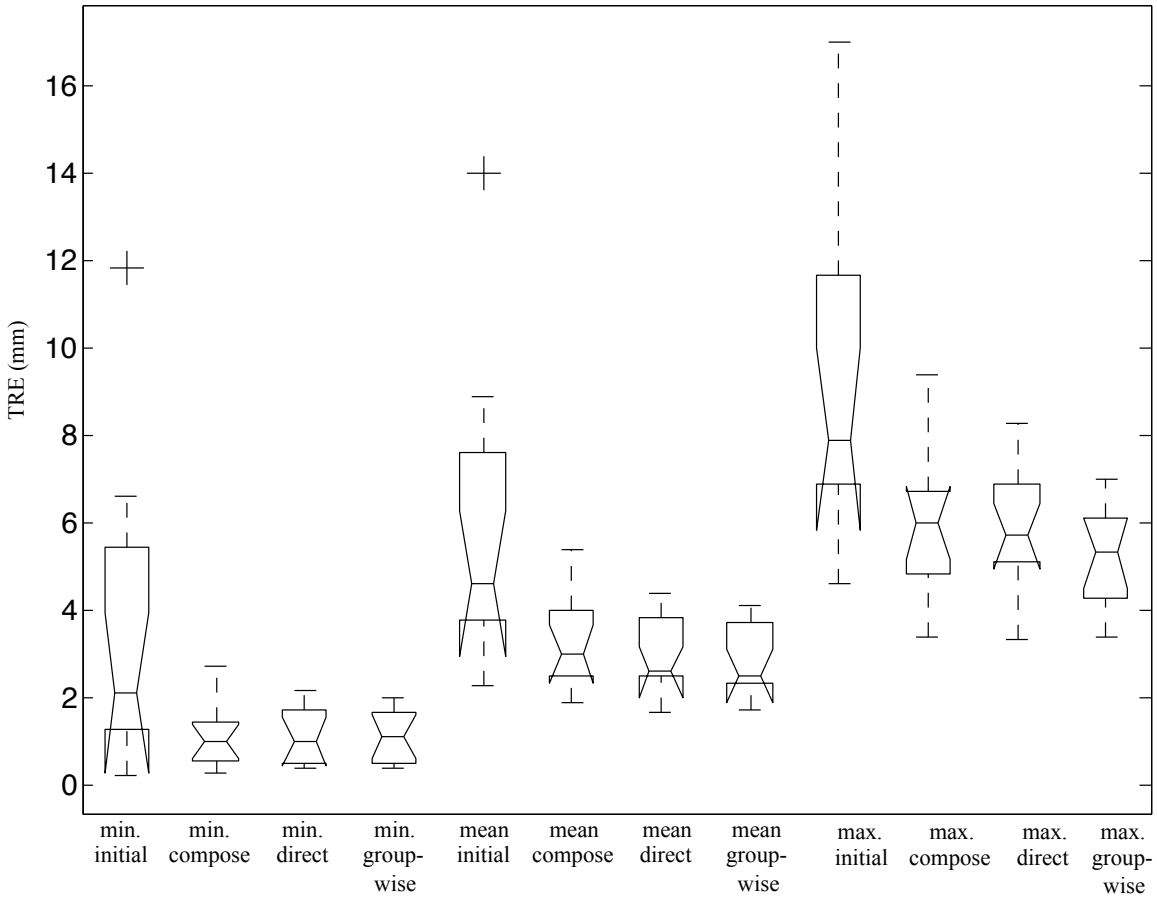

Fig. 7: The minimum, mean and maximum TRE values of Table 2 before and after registration using the three different registration techniques to estimate $\mathbf{T}_{1\leftarrow 3}$.

Acknowledgements: The authors would like to thank anonymous reviewers for their constructive feedback. This work was financed by the Fonds Québécois de la recherche sur la nature et les technologies, the Canadian Institute of Health Research (MOP-97820), and the Natural Science and Engineering Research Council of Canada. H. Rivaz is supported by a post-doctoral fellowship from the Natural Sciences and Engineering Research Council of Canada.

Conflict of interest: None

References

1. D. Hill, C. Maurer, R. Maciunas, J. Barwise, M. Fitzpatrick, and M. Wang, "Measurement of intraoperative brain surface deformation under a craniotomy," *Neurosurgery*, vol. 43, no. 3, pp. 514–526, 1998.
2. D. Roberts, A. Hartov, F. Kennedy, M. Miga, and K. Paulsen, "Intraoperative brain shift and deformation: A quantitative analysis of cortical displacement in 28 cases," *Neurosurgery*, vol. 43, no. 4, pp. 749–758, 1998.
3. S. Ji, X. Fan, A. Hartov, D. W. Roberts, and K. D. Paulsen, "Estimation of intraoperative brain deformation," in *Soft Tissue Biomechanical Modeling for Computer Assisted Surgery*. Springer, 2012, pp. 97–133.
4. D. Kuhnt, M. H. Bauer, and C. Nimsky, "Brain shift compensation and neurosurgical image fusion using intraoperative mri: current status and future challenges," *Critical Reviewsł in Biomedical Engineering*, vol. 40, no. 3, 2012.
5. A. Nabavi, P. Black, and et al., "Serial intraoperative magnetic resonance imaging of brain shift," *Neurosurgery*, vol. 48, no. 4, pp. 787–798, 2001.
6. C. Nimsky, A. Fujita, O. Ganslandt, B. Von Keller, and R. Fahlbusch, "Volumetric assessment of glioma removal by intraoperative high-field magnetic resonance imaging," *Neurosurgery*, vol. 55, no. 4, pp. 358–370, 2004.
7. C. Truwit, A. J. Martin, and W. A. Hall, "MRI guidance of minimally invasive cranial applications," in *Interventional Magnetic Resonance Imaging*. Springer, 2012, pp. 97–112.
8. M. Giordano, V. M. Gerganov, H. Metwali, R. Fahlbusch, A. Samii, M. Samii, and H. Bertalanffy, "Feasibility of cervical intramedullary diffuse glioma resection using intraoperative magnetic resonance imaging," *Neurosurgical review*, vol. 37, no. 1, pp. 139–146, 2014.
9. M. Czyż, P. Tabakow, A. Weiser, B. Lechowicz-Głogowska, L. Zub, and W. Jarmundowicz, "The safety and effectiveness of low field intraoperative mri guidance in frameless stereotactic

biopsies of brain tumoursdesign and interim analysis of a prospective randomized trial," *Neurosurgical review*, vol. 37, no. 1, pp. 127–137, 2014.

10. B. Sommer, P. Grummich, R. Coras, B. S. Kasper, I. Blumcke, H. M. Hamer, H. Stefan, M. Buchfelder, and K. Roessler, "Integration of functional neuronavigation and intraoperative mri in surgery for drug-resistant extratemporal epilepsy close to eloquent brain areas," *Neurosurgical focus*, vol. 34, no. 4, p. E4, 2013.
11. P. Black, F. A. Jolesz, and K. Medani, "From vision to reality: the origins of intraoperative mr imaging," in *Intraoperative Imaging*. Springer, 2011, pp. 3–7.
12. G. Keles, K. Lamborn, and S. Berger, "Coregistration accuracy and detection of brain shift using intraoperative sononavigation during resection of hemispheric tumors," *Neurosurgery*, vol. 53, pp. 556–562, 2003.
13. A. Unsgaard, T. Selbekk, S. Gronningsaeter, S. Ommedal, and H. Nagelhus, "Ability of navigated 3D ultra- sound to delineate gliomas and metastases: Comparison of image interpretations with histopathology," *Acta Neurochirurgica*, vol. 147, no. 4, pp. 1259–1269, 2005.
14. M. Letteboer, P. Willems, M. Viergever, and W. Niessen, "Brain shift estimation in image-guided neurosurgery using 3-d ultrasound," *IEEE Trans Med. Imag.*, vol. 52, pp. 267–276, 2005.
15. O. Rygh, T. Selbekk, S. Torp, S. Lydersen, T. Hernes, and G. Unsgaard, "Comparison of navigated 3D ultrasound findings with histopathology in subsequent phases of glioblastoma resection," *Acta Neurochirurgica*, vol. 150, no. 10, pp. 1033–1042, 2005.
16. D. Miller, L. Benes, and U. Sure, "Stand-alone 3d-ultrasound navigation after failure of conventional image guidance for deep-seated lesions," *Neurosurgical review*, vol. 34, no. 3, pp. 381–388, 2011.
17. S. Ji, X. Fan, D. W. Roberts, A. Hartov, and K. D. Paulsen, "Optimizing nonrigid registration performance between volumetric true 3d ultrasound images in image-guided neurosurgery," in *SPIE Medical Imaging*. International Society for Optics and Photonics, 2011, pp. 79 640V–79 640V.
18. S. Ji, D. W. Roberts, A. Hartov, K. D. Paulsen *et al.*, "Intraoperative patient registration using volumetric true 3d ultrasound without fiducials," *Medical physics*, vol. 39, no. 12, p. 7540, 2012.
19. L. Mercier, V. Fonov, C. Haegelen, R. Maesstro, K. Petrecca, and D. L. Collins, "Comparing two approaches to rigid registration of three-dimensional ultrasound and magnetic resonance images for neurosurgery," *Compt Aided Surg*, vol. 7, no. 1, pp. 125–136, 2012.
20. T. Selbekk, A. S. Jakola, O. Solheim, T. F. Johansen, F. Lindseth, I. Reinertsen, and G. Unsgård, "Ultrasound imaging in neurosurgery: approaches to minimize surgically induced image artefacts for improved resection control," *Acta neurochirurgica*, vol. 155, no. 6, pp. 973–980, 2013.
21. I. Reinertsen, A. Jakola, P. Friderichsen, F. Lindseth, O. Solheim, T. Selbekk, and G. Unsgård, "A new system for 3d ultrasound-guided placement of cerebral ventricle catheters," *International journal of computer assisted radiology and surgery*, vol. 7, no. 1, pp. 151–157, 2012.
22. L. Mercier, R. F. Del Maestro, K. Petrecca, D. Araujo, C. Haegelen, and D. L. Collins, "Online database of clinical mr and ultrasound images of brain tumors," *Medical Physics*, vol. 39, p. 3253, 2012.
23. X. Fan, S. Ji, K. Fontaine, A. Hartov, D. Roberts, and K. Paulsen, "Simulation of brain tumor resection in image-guided neurosurgery," in *SPIE Medical Imaging*. International Society for Optics and Photonics, 2011, pp. 79 640U–79 640U.
24. X. Fan, S. Ji, A. Hartov, D. Roberts, and K. Paulsen, "Retractor-induced brain shift compensation in image-guided neurosurgery," in *SPIE Medical Imaging*. International Society for Optics and Photonics, 2013, pp. 86 710K–86 710K.
25. H. Rivaz, E. M. Boctor, M. A. Choti, and G. D. Hager, "Ultrasound elastography using multiple images," *Medical image analysis*, vol. 18, no. 2, pp. 314–329, 2014.
26. H. Rivaz and D. L. Collins, "Near real-time robust nonrigid registration of volumetric ultrasound images for neurosurgery," *Ultrasound in Medicine and Biology*, in press.
27. H. Rivaz, S. Chen, and D. L. Collins, "Automatic deformable mr-ultrasound registration for image-guided neurosurgery," *IEEE Trans. Medical Imaging*, 2015.
28. A. Roche, X. Pennec, G. Malandain, and N. Ayache, "Rigid registration of 3-d ultrasound with mr images: a new approach combining intensity and gradient information," *IEEE Trans Med Imag*, vol. 20, no. 72, pp. 291–237, 2001.
29. T. Arbel, X. Morandi, R. Comeau, and D. L. Collins, "Automatic non-linear mri-ultrasound registration for the correction of intraoperative brain deformations," *Compt Aided Surg*, vol. 9, no. 4, pp. 123–136, 2004.
30. D. L. Collins, P. Neelin, T. M. Peters, and A. C. Evans, "Automatic 3d intersubject registration of mr volumetric data in standardized talairach space," *Journal of computer assisted tomography*, vol. 18, no. 2, pp. 192–205, 1994.
31. M. Kuklisova-Murgasova, A. Cifor, R. Napolitano, A. Papageorghiou, G. Quaghebeur, M. A. Rutherford, J. V. Hajnal, J. Alison Noble, and J. A. Schnabel, "Registration of 3d fetal neurosonography and mri," *Medical Image Analysis*, 2013.
32. G. Penney, J. Blackall, M. Hamady, T. Sabharwal, A. Adam, and D. Hawks, "Registration of freehand 3d ultrasound and magnetic resonance liver images," *Med Imag Anal*, vol. 8, no. 1, pp. 81–91, 2004.
33. S. Ji, Z. Wu, A. Hartov, D. Roberts, and K. Paulsen, "Mutual-information-based image to patient re-registration using intraoperative ultrasound in image-guided neurosurgery," *Med. Phys.*, vol. 35, no. 10, pp. 4612–4624, 2008.
34. A. Hartov, D. W. Roberts, and K. D. Paulsen, "A comparative analysis of coregistered ultrasound and magnetic resonance imaging in neurosurgery," *Neurosurgery*, vol. 62, no. 3, pp. 91–101, 2008.
35. R. Brooks, D. L. Collins, X. Morandi, and T. Arbel, "Deformable ultrasound registration without reconstruction," in *Medical Image Computing and Computer-Assisted Intervention–MICCAI 2008*. Springer, 2008, pp. 1023–1031.
36. W. Zhang, M. Brady, H. Becher, and A. Noble, "Spatio-temporal (2d+t) non-rigid registration of real-time 3d echocardiography and cardiovascular mr image sequences," *Physics Med Biol*, vol. 56, pp. 1341–1360, 2011.
37. J. Kybic and M. Unser, "Fast parametric elastic image registration," *IEEE Trans. Med. Imag.*, vol. 12, pp. 1427–1442, 2003.
38. H. Rivaz, E. M. Boctor, M. A. Choti, and G. D. Hager, "Real-time regularized ultrasound elastography," *Medical Imaging, IEEE Transactions on*, vol. 30, no. 4, pp. 928–945, Apr 2011.
39. P. Jannin, J. M. Fitzpatrick, D. J. Hawkes, X. Pennec, R. Shahidi, and M. W. Vannier, "Validation of medical image processing in image-guided therapy," *Neurosurgery*, vol. 21, no. 2, pp. 1445–1449, 2002.